PHILOSOPHICAL TRANSACTIONS OF THE ROYAL SOCIETY A MATHEMATICAL, PHYSICAL & ENGINEERING SCIENCES

Thin–film trilayer manganate junctions

Sun J. Z.

Phil. Trans. R. Soc. Lond. A 1998 **356**, 1693-1712
doi: 10.1098/rsta.1998.0242

The Royal Society

Thin-film trilayer manganate junctions

By J. Z. Sun

IBM T. J. Watson Research Center, PO Box 218, Yorktown Heights, NY 10598, USA

Spin-dependent conductance across a manganate–barrier–manganate junction has recently been demonstrated. The junction is a $La_{0.67}Sr_{0.33}MnO_3$–$SrTiO_3$–$La_{0.67}Sr_{0.33}MnO_3$ trilayer device supporting current-perpendicular transport. Large magnetoresistance of up to a factor of five change was observed in these junctions at 4.2 K in a relatively low field of the order of 100 Oe. Temperature and bias dependent studies revealed a complex junction interface structure whose materials physics has yet to be understood.

Keywords: manganite; low-field magnetoresistance; trilayer functions; spin-dependent transport; tunnelling

1. Introduction

Since the discovery of large magnetoresistance (MR) in $La_{0.67}Ba_{0.33}MnO_3$ at room temperature, epitaxial thin films (Helmolt *et al*. 1993), there has been a resurgence of interest in doped perovskite manganate compounds. Doped perovskite manganates in this case refers to the family of materials related to compounds with a chemical composition of $A_{1-x}B_xMnO_3$, where A stands for trivalent rare-earth elements such as La, Pr, etc., and B stands for divalent alkaline-earth elements, such as Ba, Sr, etc. Materials refinements have revealed that very large magnetoresistances, of over three orders of magnitude change in resistance, can be observed in such compounds prepared through special heat treatment (Jin *et al*. 1994*a*, *b*; McCormack *et al*. 1994). These materials have since been referred to as colossal magnetoresistance, or CMR materials. The large magnetoresistance effect in these compounds was referred to as CMR effect.

The physics of CMR is complex due to the similar energy scales involved for interactions among the lattice, electronic and magnetic degrees of freedom. The basic electronic interactions in these materials were investigated back in the 1950s. The double-exchange model (Anderson & Hasegawa 1955; de Gennes 1960) was proposed to explain the simultaneous onset of metallic conductivity and ferromagnetism as doping concentration x is increased across the insulator–metal transition point of $x \sim 0.2$. It was also then understood that there is a strong correlation between the Mn–O–Mn bond length and bond angle and the magnetic coupling of adjacent Mn ions (Goodenough *et al*. 1961). A Jahn–Teller distortion lifts the double-degeneracy of the e_g orbitals of Mn d-electrons, and provides a mechanism for strong coupling between the electronic, magnetic and lattice degrees of freedom. In bulk ceramic materials, a Jahn–Teller distortion-related orthorhombicity is present in $La_{1-x}Ca_xMnO_3$ in the doping range of $0 \leqslant x \leqslant 0.2$ (Wollan & Koehler 1955). Above $x = 0.2$, such a static distortion of the lattice is no longer observable.

To explain the CMR effect, it was recently proposed that, even for $x > 0.2$, dynamically fluctuating local Jahn–Teller distortion still exists, which provides a mechanism for the localization of ferromagnetic polarons (Millis *et al*. 1996; Roder *et al*. 1996; Millis 1996). For CMR materials at $x \sim 0.3$ in temperatures above the Curie point T_C, these polarons are localized. Electrical conduction occurs via the hopping process. For temperatures well below T_C, on the other hand, the electornic states appear more extended, and a band-like conduction is more appropriate. Local spin-density approximation calculations (Pickett & Singh 1996) have been carried out for $La_{1-x}Ca_xMnO_3$ in the region $x = \frac{1}{4} \sim \frac{1}{3}$. Their results suggest an almost completely spin-polarized Mn d-band. Therefore, these materials may behave as half-metals at temperatures below T_C, and hence may exhibit a large spin-dependent conductance across a tunnelling barrier (Slonczewski 1976).

For magnetic field-sensing applications, low-field responsivity is necessary. Large MR is desired in field ranges of tens to hundreds of Oe. This presents a challenge for CMR materials, since the CMR effect observed in the generic doped manganate perovskites involves a magnetic field above 1 T (Jin *et al*. 1994*a*; Helmolt *et al*. 1993), and the low-field magnetoresistance in the field range 10–100 Oe remains minimal.

One might expect large spin-dependent conductivity across a macroscopic interface, between two CMR electrodes across which the magnetization abruptly changes direction. This may be due either to local spin-dependent hopping, as prescribed by the double-exchange mechanism, or to spin-dependent tunnelling, if the interface is electrically insulating enough to behave as a tunnelling barrier. Such a macroscopic interface disrupts the magnetic exchange-coupling, so that the easy rotation of the magnetic moment from one electrode to the other can be obtained.

Three approaches have been taken to experimentally exploit this concept. The first approach is to use a crystalline grain-boundary as the interface, and study the spin-dependent transport across. The role of grain boundary in providing additional contributions to low-field magnetoresistance has long been suspected (Ju *et al*. 1995; Gupta *et al*. 1996; Hwang *et al*. 1996). Direct experimental observation of grain-boundary-originated magnetoresistance has recently been made (Mathur *et al*. 1997; Steenbeck *et al*. 1997) which shows a 30% magnetoresistance in a field of less than 500 Oe.

The second approach used the naturally occurring interplanar conductivity in the two-dimensional version of the CMR material $La_{1.4}Sr_{1.6}Mn_2O_7$ (Kimura *et al*. 1996) with magnetoresistance of 240% in less than 500 Oe at 4.2 K, using the layered single crystal compound of $La_{2-2x}Sr_{1+2x}Mn_2O_7$ at $x = 0.3$. The transport direction was perpendicular to the planes of layering, and the authors argued that transport in this direction may be due to spin-dependent tunnelling.

The third approach makes use of thin film trilayer junctions, fabricated from epitaxial trilayer films to support current-perpendicular (CPP) transport. Successful demonstration of large low-field magnetoresistance in CMR-based devices was first realized in such junctions (Sun *et al*. 1996; Lu *et al*. 1996). The devices are lithographically fabricated from $La_{0.67}(Ca,Sr)_{0.33}MnO_3$–$SrTiO_3$–$La_{0.67}(Ca,Sr)_{0.33}MnO_3$ (LSMO-STO–LSMO, or LCMO–STO–LCMO) trilayer epitaxial thin films. The junctions show large low field magnetoresistance, of about a factor of two to five, in a field around 100 Oe at 4.2 K. These results provide an existence proof that low-field CMR is possible.

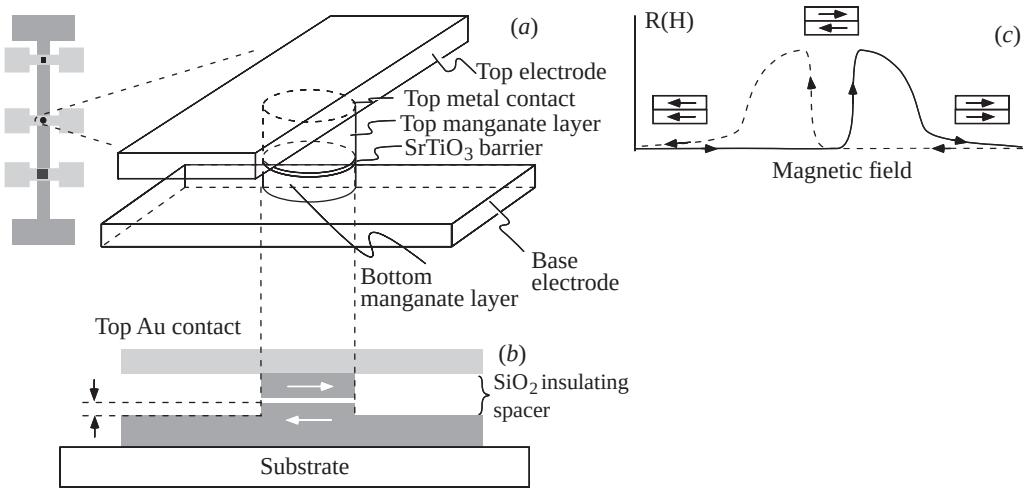

Figure 1. A schematic view of the LSMO–barrier–LSMO trilayer thin film junction structure. (*a*) Top-view of the device (left); three-dimensional illustration of the current-perpendicular pillar structure (right). (*b*) Side-view of the structure, showing the over-etch step which adds additional magnetic coupling between the top and bottom ferromagnetic electrodes. (*c*) Junction resistance as a function of sweeping magnetic field, showing the transitions from parallel to antiparallel to parallel state of the magnetic moment alignments of the electrodes. Figure reproduced from Sun (1997).

This paper focuses on experimental issues concerning spin-dependent transport in CMR trilayer junctions.

2. Structure of a thin film trilayer junction

(*a*) *Conceptual design of the device*

A typical structure for thin film trilayer magnetic junction is illustrated in figure 1. The junction comprises a top and a bottom magnetic electrode, made of epitaxial CMR thin films. The two electrodes are separated by a thin layer of foreign material, such as $SrTiO_3$, which disrupts the magnetic exchange-coupling between the electrodes, and makes it possible to macroscopically rotate the magnetic moment of one electrode with respect to the other. Transport current is forced to flow perpendicularly to the barrier in the CPP geometry. If the barrier is thin enough, it will allow some passage of electrical current, either via metal–insulator–metal tunnelling, or by some other more complex and inhomogeneous processes, such as defect-assisted hopping through the barrier. One hopes to directly observe spin-dependent transport across the barrier. By spin-dependent transport we mean that, on a macroscopic scale, the conductance across the barrier is dependent on the relative orientation of the ferromagnetic (FM) moments of the two electrodes. Usually, the transport resistance across such a structure would be minimum when the moments of the two FM electrodes are parallel, and maximum when they are antiparallel. This is true in many mechanisms including spin-dependent tunnelling, double-exchange-mediated nearest-neighbour hopping, or in metallic, two-channel, spin-scattering limited conduction.

When such a trilayer is subjected to an applied magnetic field, the junction resistance will show a particular type of field dependence. The junction stays in its low resistance state in a sufficiently high field. But when the applied field is swept from its negative value to positive, one electrode will magnetically rotate before the other if the device is designed such that the two electrodes have different magnetic anisotropy. This will result in a momentary antiparallel arrangement of the relative moments across the barrier, and the junction resistance will register its high value in this field range. This is schematically illustrated in figure 1*c*.

The conduction mechanism across the barrier layer can vary. In metal or alloy-based thin film trilayers, several types of separation layers have been experimented with. The separation layer can be either a non-magnetic metal, as in the case of a spin-valve (Dieny *et al*. 1991), or an insulator, as in spin-dependent tunnelling (Slonczewski 1976, 1989; Julliere 1975). Spin-dependent tunnelling has been observed in elemental and alloy ferromagnetic metal electrode systems (Julliere 1975; Meservey & Tedrow 1993; Moodera *et al*. 1995; Matsuyama *et al*. 1995; Miyazaki & Tezuka 1995*a*, *b*; Gallagher *et al*. 1996; Platt *et al*. 1996). There are still debates as to whether such a type of tunnelling should be observable in d-band dominant CMR materials (Zhang & Levy, personal communication), since d-electrons decay much more rapidly into the barrier than s-electrons (Chazalviel & Yafet 1977; Hertz & Aoi 1973).

For CMR trilayers, the most commonly used barrier material is a thin layer of epitaxial $SrTiO_3$ film, 20–50Å thick. The role of this barrier material is yet to be fully understood, as will be discussed later.

Nonlinear current–voltage characteristics have been observed in CMR–barrier–CMR junctions (Sun *et al*. 1996, 1997; Lu *et al*. 1996). These current–voltage (I–V) characteristics appear roughly consistent with a metal–barrier–metal tunnelling process. However, the nonlinear I–V characteristic alone is insufficient for establishing a tunnelling transport mechanism, and other mechanisms have also been known to give rise to nonlinear I–Vs (Maekawa *et al*. 1996; Asano *et al*. 1993, 1994). The exact conduction mechanism in these CMR junctions remains unclear at present.

(*b*) *Fabrication*

In our laboratory, thin film trilayers were made by using epitaxial $La_{0.67}Sr_{0.33}MnO_3$ (LSMO) electrodes and $SrTiO_3$ (STO) barriers (Lu *et al*. 1996; Sun *et al*. 1996, 1997). Briefly, epitaxial growth was achieved by using *in situ* pulsed-laser deposition. Typical growth conditions included a substrate temperature of 600 to 800 °C, and an oxygen pressure of 300 mTorr. A Nd-YAG laser was used in its frequency tripled mode (355 nm) at 10 Hz repetition. The laser intensity on target surface was estimated to be around 3–5 J cm^{-2}. Deposition was done using the sequence of 600 Å LSMO, followed by 20–50 Å of STO, followed again by 400 Å of LSMO. Typical deposition rate for LSMO was around 2.6 Å s^{-1}, STO about 1.8 Å s^{-1}. Single crystal substrates of $SrTiO_3$ (1 0 0), $LaAlO_3$ (1 0 0) and $NdGaO_3$ (1 1 0) have all been used for experimentation. After deposition, the substrate was cooled in 300 Torr of oxygen to room temperature in about 1 h. A thin layer of silver, typically 500 Å or less, was sputter-deposited to the surface of the trilayer before it was taken out of the vacuum system for further processing.

Structurally, on the local scale of several thousand angstroms at least, the LSMO–STO–LSMO interfaces are well-formed, and are free of gross defects. The continua-

Figure 2

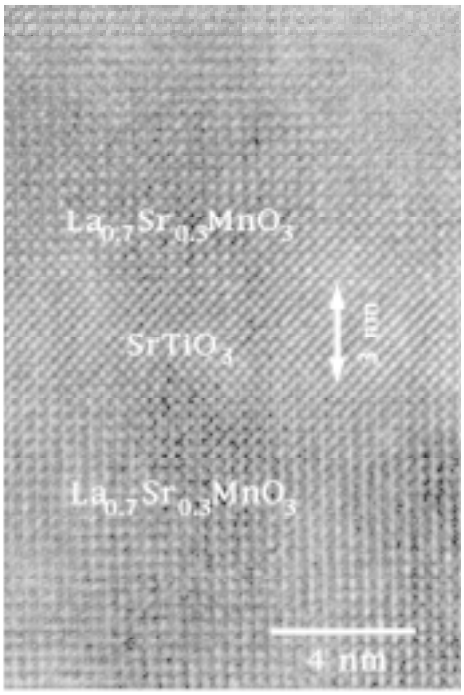

Figure 3

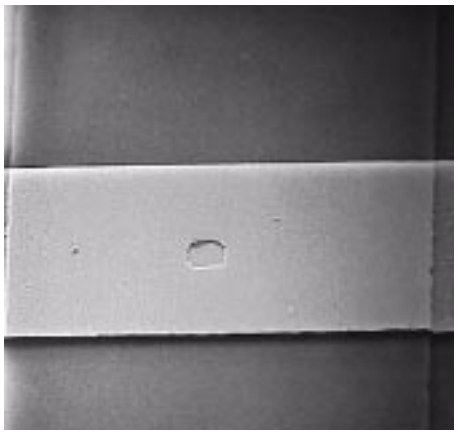

Figure 2. A cross-section transmission electron micrograph showing the epitaxial registration of lattice fringes between the LSMO electrodes and the STO barrier layer. Figure reproduced from Lu *et al*. (1996).

Figure 3. A SEM micrograph of a manganate trilayer device. The centre junction size is $2\times4\ \mu m^2$. The slightly jagged edges are due to lift-off of the SiO_2 insulation layer. Shape of the actual junction pillar is better defined than what can be seen.

tion of epitaxial growth of LSMO across the STO barrier layer is confirmed by X-ray diffraction as well as by cross-sectional transmission electron microscopy (TEM). A representative TEM picture of the trilayer interface is shown in figure 2, in which case a coherent lattice fringe can be seen to carry across the STO barrier layer from the bottom LSMO to the top.

Optical photolithography was used to fabricate CPP junctions from trilayers. The shape of the base-electrode layer was formed first, by ion milling through a photoresist stencil. Ion milling was done by using neutralized Ar ions, 500 eV, 0.3 mA cm^{-2}, 45° incidence angle. After stripping the resist, a second resist pattern was put on, which defined the pillar structure forming the junctions. Again ion milling was used, in this case to etch halfway into the film, timed to stop immediately past the STO barrier layer, forming the pillar structure from the trilayers. A blanket SiO_2 layer, typically about 3000 Å thick, was then sputter-deposited on top, followed by a lift-off step that removes the resist layer from on top of the pillars, opening up self-aligned holes for top metallic contact. A layer of about 2000 Å sputtered gold was used for top contact, which was subsequently etched using yet another level of photoresist step, forming the cross-bar structure from which 4-probe measurements could be

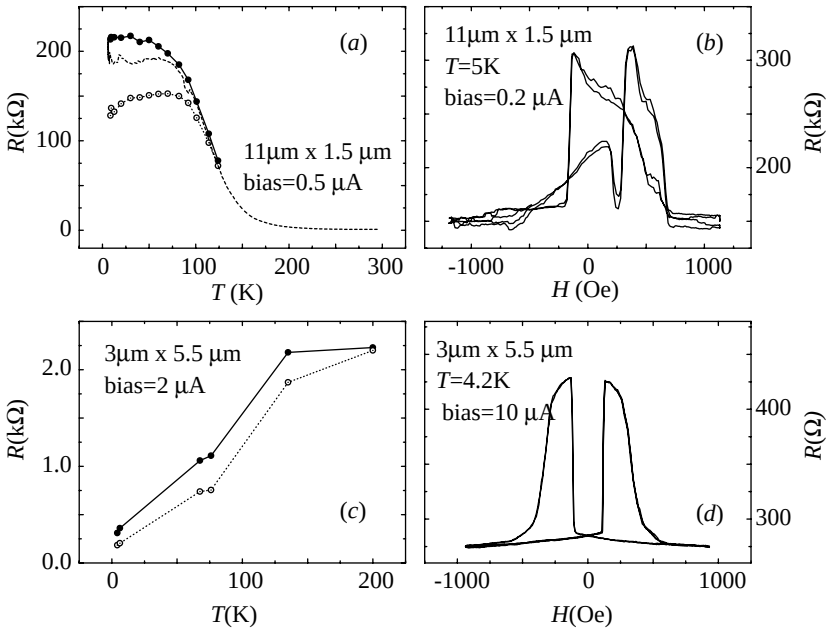

Figure 4. Two types of junction behaviour under varying temperature and magnetic field. (*a*) High resistance junction. Resistance increases with decreasing temperature; large magnetoresistance at low temperature. The two branches of curves show the resistive-low and -high states of the junction. Dashed line is zero-field cooling results. (*b*) Resistance versus field loops of a high resistance junction, showing complex switching behaviour. (*c*) Low-resistance junction, resistance tends to decrease with decreasing temperature. (*d*) Field dependence of a low-resistance junction. Figure reproduced from Sun (1997).

made of individual junction pillars underneath each gold contact bridge. A scanning electron micrograph (SEM) of a typical device structure made with this process is shown in figure 3. To make certain there was no interdiffusion-related insulation problem between SiO_2 and gold, as well as for promoting adhesion, a thin layer of titanium, usually about 20–50 Å thick, was put down between the SiO_2 and the top gold layer. The quality of SiO_2 insulation was further confirmed by the consistency between results from devices fabricated using an MgO insulation layer and from devices made by using SiO_2.

3. Transport properties

(*a*) *Overview*

Two types of junction behaviour were observed. They can be classified according to their temperature dependence. Figure 4 presents a summary. In one type of junctions, typically with STO barriers on the thicker side (30–50 Å), the junction resistance increases with decreasing temperature, as shown in figure 4*a*. These typically involve junctions of sizes below 10 μm, and are devices with the largest observed magnetoresistance at low temperatures. For this type of junction, the magnetic field dependence of junction resistance, $R(H)$, tends to be rather complex, an example is shown in figure 4*b*.

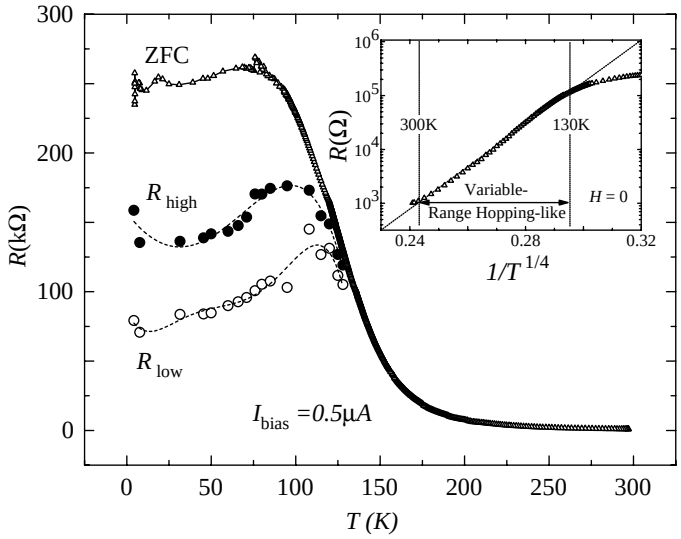

Figure 5. Temperature dependence of an LSMO–STO–LSMO junction. We noticed that for some junctions such as this one, the initial zero-field cooled trace gives a higher resistance value at low temperature than subsequent measurement cycles. Inset: junction resistance plotted to show the $T^{1/4}$ scaling relation in the high temperature region between 130 K and room temperature. Figure reproduced from Sun *et al*. (1997).

Another type of junction, typically involving thinner STO barriers (below 30 Å), shows a decreasing junction resistance upon the lowering of sample temperature. These junctions often have cleaner, more reproducible $R(H)$ loops, as shown in figure 4*d*. The interpretation of data from these low-resistance junctions is tricky, because the junction resistance could approach the base-electrode's sheet resistance. For a 600 Å LSMO base electrode with resistivity of 10^{-4}–$10^{-3}\,\Omega\,\mathrm{cm}$ at 4.2 K, we have a base-electrode $R_{\square} \approx 15$ to $150\,\Omega$. When junction resistance approaches that of $R_{\square}$, distributed voltage drop in the base electrode can no longer be ignored, and one has to be careful in distinguishing between true junction resistance and the apparent resistance caused by voltage distribution inside the base electrode (Pedersen & Vernon 1967). Such artifacts can cause a superficially high value of magnetoresistance (Moodera *et al*. 1996).

Another difficulty in studying low-resistance junctions has to do with sample heating. It is difficult to apply a large voltage across a low resistance junction without significantly heating up the *junction area* of the sample. Perovskites such as $SrTiO_3$ have relatively low thermal conductivity (around $10\,\mathrm{W\,K^{-1}\,m^{-1}}$ for STO at room temperature, compared to about $144\,\mathrm{W\,K^{-1}\,m^{-1}}$ for single crystal silicon, for example. $NdGaO_3$ single crystal substrates have probably even lower thermal conductivity). Therefore, sample heating can be significant on a local scale for the junction, even when the input power is insufficient to cause much observable heating over the chip). For these two reasons, most of our discussions will be focused on devices of the first type, namely the high resistance junctions whose resistance increases upon cooling of the sample, and whose resistance value is at least an order of magnitude larger than the base-electrode $R_{\square}$.

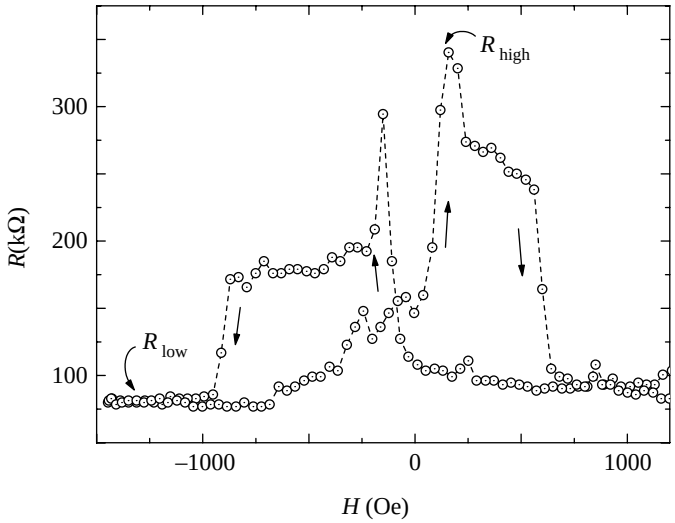

Figure 6. Magnetic field dependence of junction resistance at 4.2 K, showing pronounced low-field spin-dependent behaviour. A maximum resistance change by about a factor of 5 is observed in this junction. The magnetic field in this measurement was swept at the frequency of 1.321 Hz. Figure reproduced from Sun *et al.* (1997).

(*b*) *Temperature dependence of junction resistance*

A representative temperature dependence of junction resistance is shown in figure 5. Two regions of temperatures involving distinctively different junction behaviour can be identified. In the first region, typically between 130 K and 300 K, the junction resistance rises almost exponentially upon the decreasing of temperature, resembling a $T^{1/4}$ scaling relation commonly seen in systems exhibiting variable range-hopping (Mott 1969). A replot of the junction resistance versus temperature data according to the scaling relation $R(T) = R_{\rm o}\exp[(T^*/T)^{1/4}]$ is shown in the inset of figure 5. In this region the magnetoresistance is minimal, typically less than 0.5% for a field sweep of couple of hundred Oe.

Below 130 K, the junction enters its second region, where the junction resistance is less sensitive to temperature variation. It becomes more noisy, and exhibits large magnetic field-exposure history dependence. This is the temperature region where large low-field magnetoresistance is observed. An example is shown in figure 6, where the junction resistance is measured as a function of sweeping magnetic field at a constant temperature of 4.2 K. Such a response to sweeping magnetic field is expected conceptually from the simple two-FM-electrode junction picture as shown in figure 1*c*. Details about the shape of the $R(H)$ loops will be discussed in the next section, here we merely use figure 6 to point out that the low-field magnetoresistance is large. For the junction shown here, a factor of 5 change in resistance is observed at a switching field of around 100 Oe at 4.2 K. This is the first observation of large MR at low-fields in CMR materials, proving that CMR is not a phenomenon limited to high magnetic fields.

We define two resistance values from data such as shown in figure 6, namely $R_{\rm high}$ and $R_{\rm low}$, corresponding to the DC resistive high- and low-state of the junction. The

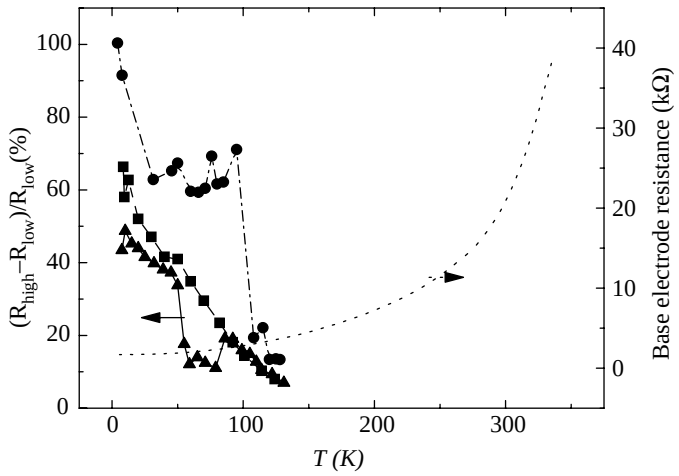

Figure 7. Temperature dependence of magnetoresistance of some CPP junctions. Right: temperature dependence of the base-electrode's resistivity. Figure reproduced from Sun (1997).

magnetoresistance contrast can then be conveniently defined as

$$C_{\mathrm{R}} = (R_{\mathrm{high}} - R_{\mathrm{low}})/R_{\mathrm{low}},$$

according to the conventions used in literature. The temperature dependences of R_{high}, R_{low} and C_{R} are shown in figures 4, 5 and 7. As mentioned above, the magnetoresistance decreases with increasing temperature, and it disappears around 130 K. This is well below T_{C} of the thin film material which is close to the resistance peak temperature. The resistance peak temperature of the base electrode is shown in figure 7 to be above 300 K. Separate measurements confirm the base-electrode's resistance peaks around 350–360 K. Clearly, something other than the film's T_{C} is limiting the upper temperature of the junction magnetoresistance.

The high temperature behaviour of junction resistance, as shown in figure 5, may suggest defect-assisted hopping as a possible conduction mechanism across the STO barrier. Indeed, such temperature dependence of resistance is common in oxide perovskite semiconductors having a large population of defect sites. The defect-assisted conduction process may provide additional high-temperature conduction channels that progressively shunt out the direct, spin-dependent conduction process manifested at low temperatures. For this scenario to work, the defect-assisted hopping has to have a large spin-flipping rate, because the high temperature conduction has apparently lost all spin-dependence information, judging from its minimal value of magnetoresistance.

There are other possibilities for a premature decrease of magnetoresistance. Spin-dependent transport across a trilayer is sensitive to interface magnetic states which may be different from that deep inside the film. This may be caused by a reduced magnetic coupling at the interface, by a discontinuous electronic structure, or by interface diffusion or oxygen deficiency. A different stress environment at the interface may cause change in an electrode's magnetic states. Excitation of surface magnons have also been suggested as a possible source for the suppression of magnetoresistance, both for high temperature and for elevated junction bias (Zhang *et al*. 1997).

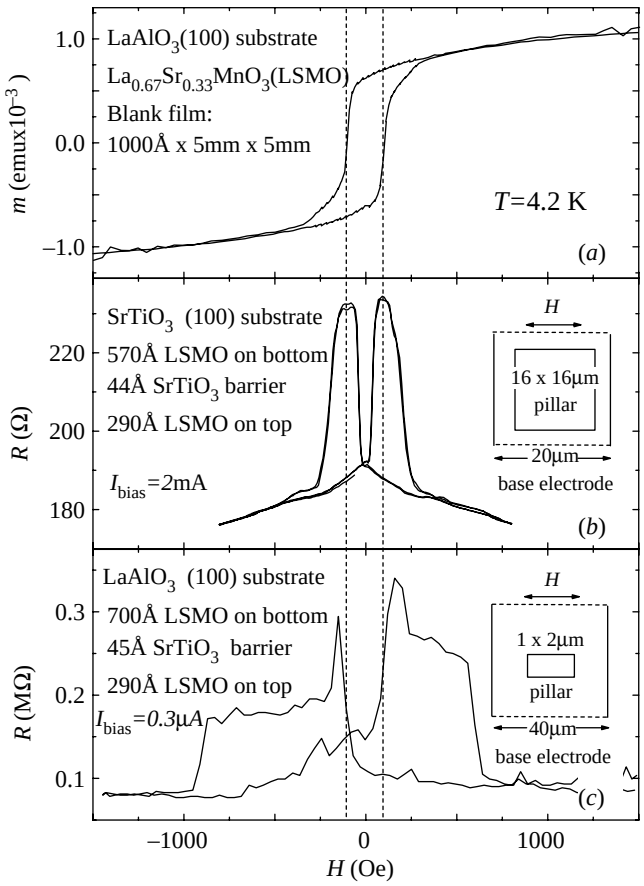

Figure 8. Comparing the $R(H)$ curves of devices to magnetic hysteresis from a blank film. (a) Magnetic hysteresis loop of a blank film. (b) $R(H)$ loop of a low-resistance junction showing a similar switching field to blank film's H_C. (c) High resistance junction. The lower switching field corresponds well to blank film's H_C, while the upper switching field is well above H_C, indicating additional magnetic interaction is present for magnetic states within the pillar. The insets in (b) and (c) show the geometry of the electrodes for the particular junctions and the relative field orientation in each case. Figure reproduced from Sun (1997).

(*c*) *Magnetic field dependence of junction resistance*

The magnetic coercivity of 33%-doped LSMO thin films is of the order of 100–200 Oe at helium temperature (Suzuki *et al*. 1997; Sun 1997). In CMR junctions, the situation is more complex. Additional magnetic interactions need to be considered. Four major contributors are: the shape anisotropy of the junction pillar, the edge coupling, the dipolar coupling across a rough junction interface, and the magnetostriction-induced anisotropy. The complexity of magnetic states in the junction pillar is apparent from our measurement such as data shown in figure 6.

Junctions with high resistance have more complex $R(H)$ loops. In figure 8, $R(H)$ loops from two junctions of different resistance are compared to the magnetic hysteresis loop of a blank film of $La_{0.67}Sr_{0.33}MnO_3$. The top panel shows a representative magnetic hysteresis loop taken on a blank $La_{0.67}Sr_{0.33}MnO_3$ epitaxial film. The mid-

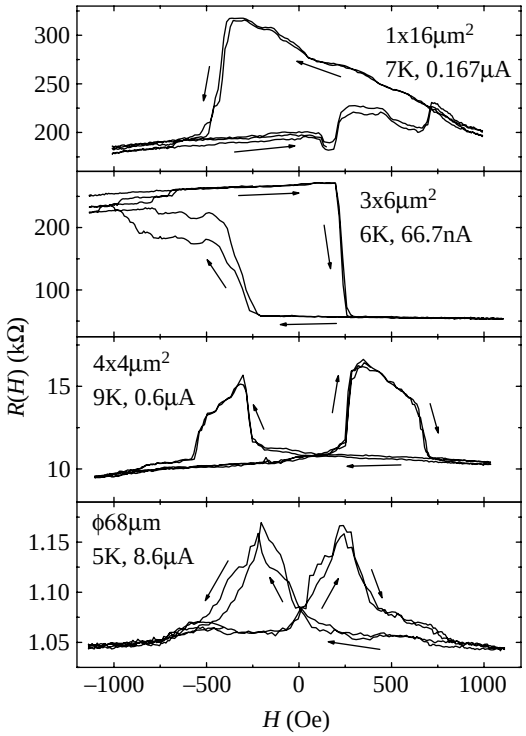

Figure 9. Some more examples of field-dependent resistance of various junctions. Junction size and measurement parameters are shown in the panels. Figure reproduced from Sun (1997).

dle panel (*b*) shows the $R(H)$ loop for a low-resistasnce junction. The switching field for this type of junction agrees well with that of the coercivity of the blank film. The lower panel (*c*) shows the $R(H)$ loop of a high-resistance junction. Here the lower switching field agrees well with the magnetic coercivity of the blank thin film. However, the upper switching field is significantly above the coercivity of the blank film. This suggests the presence of magnetic states with enhanced magnetic anisotropy, be it from shape, strain, or interface coupling. The $R(H)$ curves for high-resistance junctions are noisy and often show preferred multiple discrete resistance values, suggesting the switching of multiple magnetic domains inside the electrodes. Over the many junctions we have measured to date, a wide variety of magnetic behaviour has been seen. Figure 9 shows some other $R(H)$ loops with complex magnetic structures. Much better understanding and control of the electrode's magnetic state is necessary.

It is also possible that part of the $R(H)$ loop complexities comes from magnetic defect-sites inside the barrier, rather than from the magnetic states of the electrodes alone. Barrier-related magnetic defects have been shown in small (less than 80 nm diameter) Ni–NiO–Co junctions to cause magnetic field-dependent fluctuations that can lead to large apparent magnetoresistance at low frequencies (Doudin *et al*. 1997).

(*d*) *Bias dependence of junction resistance*

Nonlinear I–V characteristics are present in all junctions that show large magnetoresistance. Following definitions similar to that from figure 6, at a given bias current

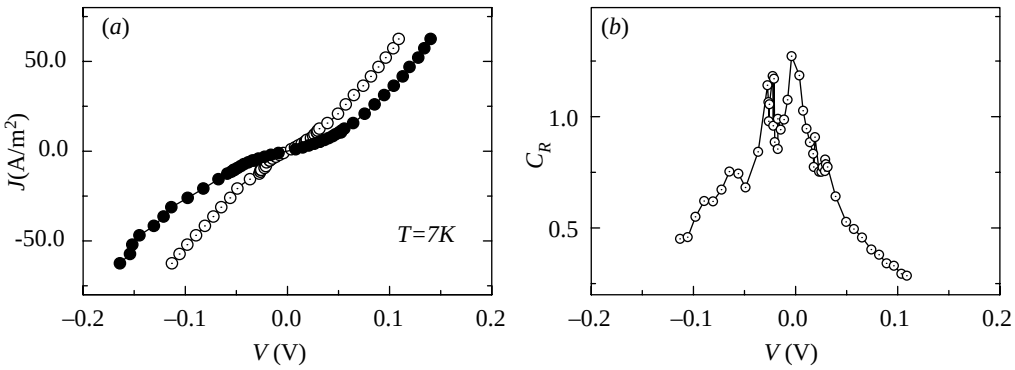

Figure 10. (*a*) Two branches of the I–V characteristics of a junction showing large magnetoresistance, corresponding to the junction's R_{high} and R_{low} state, respectively. Junction size is $11 \times 1.5\,\mu\mathrm{m}^2$. (*b*) The magnetoresistance ratio, C_{R}, as a function of junction bias voltage, showing a decrease of MR as junction bias is increased.

for a junction we define V_{high} and V_{low} as the high- and low-voltage state corresponding to R_{high} and R_{low}. We trace V_{high} and V_{low} as a function of bias current, and the resulting two branches of the I–V characteristics and the bias-dependent magnetoresistance ratio C_{R} are shown in figure 10. The two branches of I–Vs show pronounced nonlinearity. At the same time the magnetoresistance ratio shows a bias-dependence, with the contrast C_{R} decreasing as junction bias is increased. This behaviour is similar to what is observed in metal-based magnetic tunnelling junctions (Moodera *et al*. 1995), although the characteristic voltage scale for the reduction of magnetoresistance is at least a factor of 3 to 5 smaller than in the case of metal junctions such as CoFe–Al_2O_3–Co (Zhang *et al*. 1997).

The bias-dependent junction transport can be further examined by plotting the differential junction conductance as a function of bias voltage. This is shown in figure 11, where the specific differential junction conductance is plotted as a function of junction bias, showing a relatively sharp conductance minimum at low-bias riding on top of a more gradually rising high-bias conductance slope. The origin of this characteristic is not well understood. It is more complex than one would expect from a simple metal–insulator–metal tunnelling junction as the Simmons tunnelling model (Simmons 1964) would predict (dotted lines). More knowledge about the barrier and the interface states of the CMR materials is necessary.

(*e*) *Size-dependence and inhomogeneity*

CMR trilayer junctions fabricated to date show large amount of inhomogeneities. Junction conductance in most cases do not scale with junction area in any simple way. This is evident in data presented in figure 11. If the junction conductances were to scale with the area, one would expect all specific conductance curves to be roughly the same in value. Instead in figure 11 the specific conductance increases with increasing junction size. Figure 12 shows two sets of junction resistances as a function of pillar size for two rows of junctions on one chip. A clear cross-over from high junction resistance to low junction resistance can been seen as the junction dimension is increased beyond a cross-over region between 2 and 10 μm. This indicates non-uniform conduction over the junction area, where high conductance paths are small

Figure 11

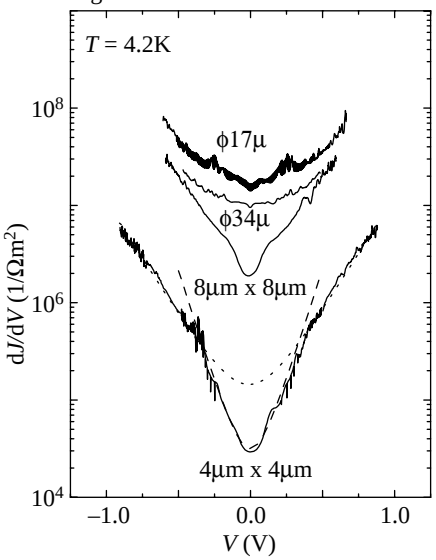

Figure 12

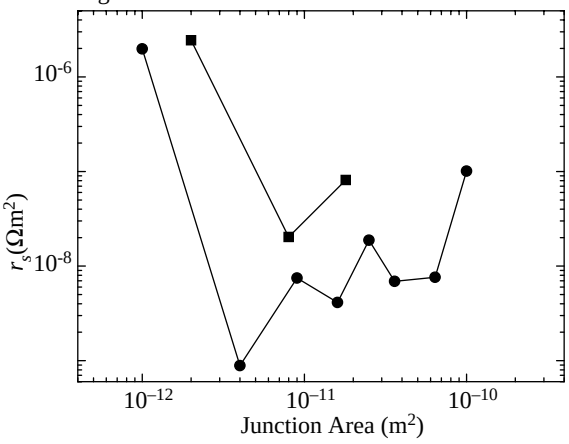

Figure 11. Bias-dependent differential conductance of LSMO–STO–LSMO junctions. The nominal barrier thickness is 39 Å. The normalized conductance decreases with decreasing junction area, suggesting inhomogeneity over a length scale of several μm. The lower conductance junctions are generally the ones that give large magnetoresistance. Notice the pronounced low-bias conductance dip. Dashed curves are Simmons model fits to the bottom curve. The low-bias fit gives $t = 30.6$ Å and $\phi = 0.703$ eV; the high-bias one gives $t = 21.6$ Å and $\phi = 1.32$ eV. These parameters should not be interpreted as a reflection of the barrier physics. The reason for this is discussed further in the later part of this section. Figure reproduced from Sun (1997).

Figure 12. Specific junction conductance as a function of junction area for different sets of junctions on the same chip. A clear break from constant conductance is seen for devices smaller than about 5 μm, indicating the presence of inhomogeneities over several microns. Similar behaviour has been seen on all chips studied.

in area compared to junction sizes, and they distribute with a mean distance on the order of 2–10 μm. Pinhole conduction is a possibility, at least for junctions of the size above the cross-over dimension.

The MR of manganate junctions appears to correlate to junction resistance. Figure 13 shows data obtained on several manganate junction chips. The junction magnetoresistance ratio C_{R} is plotted against the specific junction resistance on a log–log plot. These data appear bunched into a cone boardered on the high MR end by a line of slope 1, and on the low MR end by a line of slope of about 0.36. A slope-equal-to-1 corrlation could indicate the presence of a parallel shunt that is magnetoresistively inactive. The meaning of the lower-bound line is not clear.

The presence of inhomogeneity further complicates the nature of conduction across these CMR junctions. Although the nonlinear I–Vs from these devices can be roughly described by the Simmons tunnelling formula, it is dangerous to conclude that such fits lead to any insight of the barrier physics or the nature of the junction. Figure 14 shows a collection of the apparent barrier thickness t and barrier height ϕ extracted from fitting Simmons model to various CMR junction I–Vs obtained at 4.2 K. The values of t, ϕ appears to form a correlation defined by $t\sqrt{\phi} = \text{const}$. This apparent

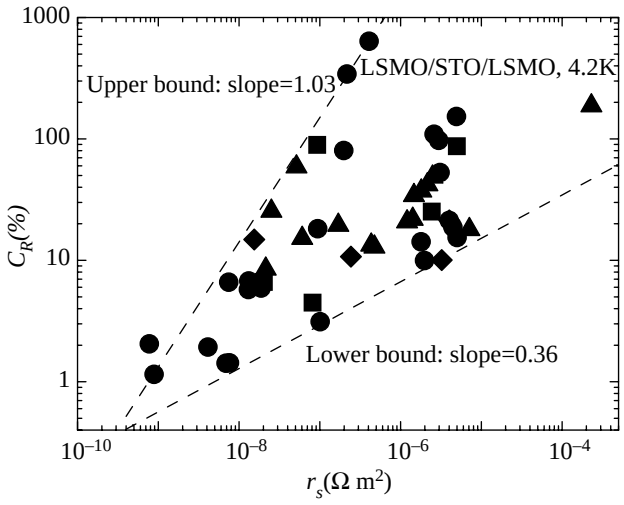

Figure 13. A summary plot of the MR of manganate junctions as a function of specific junction resistance r_s. Data were gathered from junctions on same chip as well as from different chips with varying deposition conditions and different nominal barrier thicknesses. The data fall within a cone of upper slope 1 and lower slope around 0.36. A slope 1 scaling on such plot might indicate the presence of a distribution of parallel shunt conductances that are magnetoresistively inactive, which might explain the upper bound. The slope of the lower bound is not understood.

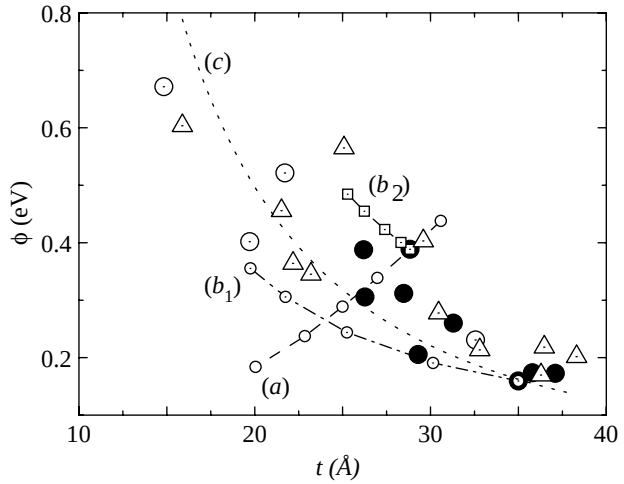

Figure 14. Fitting to Simmons's formula equation (A 1) of the 4.2 K I–V of many CMR junctions gave this distribution of the variables t, ϕ. The apparent correlation between t and ϕ is most likely due to the presence of parallel shunt conductance (if the principal nonlinear conductance does come from tunnelling). A distribution of effective area κ between 1.0 and 10^{-4} leads to a set of varying t, ϕ as shown in curve (a), which starts with $t = 28.84$ Å, and $\phi = 0.3885$ eV at $\kappa = 1$. A distribution of parallel shunt conductance by a factor of 10 causes t, ϕ to spread as illustrated in curves (b_1) and (b_2). Curve (c) is an example of a constant product of $t\phi^{1/2} = 14.1$ Å eV$^{1/2}$.

correlation as it turns out is a sure sign that we are not looking at clean tunnelling junctions but rather are just parametrizing a complex nonlinear device with a functional form of the Simmons formula. A more quantitative analysis is given in the appendix.

4. Summary and future challenges

Large low-field magnetoresistance is demonstrated in CMR trilayer junctions at temperatures below 130 K. For the first time in CMR materials system a large magnetoresistance of a factor of 5 is observed in an applied field around 100 Oe. This provides an existence proof that CMR effect can be obtained in low-fields. Nonlinear I–V characteristics and bias-dependent magnetoresistances have been observed in CMR trilayer junctions. These behaviours are qualitatively similar to what was observed in metal–insulator–metal spin-dependent tunnelling systems. Much of the physics for CMR junctions remains to be explored. The major experimental challenge is to master the materials science in the preparation of a well-controlled, well-characterized barrier interface, so that transport over the junction region could be more uniform, which will then allow more quantitative examination of the transport process.

The control of the magnetic state of the electrodes requires more study. Better control of the shape of the junction pillar is needed to assure a reproducible micromagnetic boundary condition. One particular issue is the control of the amount of over etch during the fabrication of the pillar, as illustrated in figure 1*b*. Because the over-etch step height determines to a large degree the amount of antiparallel coupling the two FM electrodes have. Also necessary is a controlled pre-setting of the magnetic easy-axis for the manganates. In most devices studied so far, the magnetic easy-axis is uncontrolled. That contributes to the observed complexity of magnetic states. Further, exchange-biasing of the manganate electrode could be looked at, since that could significantly simplify the micromagnetics of the trilayer junction structure, and make its response to applied magnetic field more predictable. The control of the magnetic state is particularly important in CMR junctions. Because of its large magnetoresistance, detailed transport study is possible only when there is a stable and well-controlled magnetic state.

The low-field magnetoresistance in trilayer CMR junctions tends to vanish at temperatures around 130–150 K, well below the Curie temperature of the electrodes, which is around 350–370 K. The reason for this is not understood at present.

From an applications point of view, one would like to extend the temperature range for large magnetoresistance. Room temperature operation of large low-field CMR has not been demonstrated at this point, although CMR effects of $C_{\mathrm{R}} \sim 60\%$ in 5 T has been seen in $La_{0.67}Ba_{0.33}MnO_3$ epitaxial thin films (Helmolt *et al*. 1993). Materials stability, device yield and compatibility to existing circuit fabrication processes are all issues that need to be resolved.

We thank Stuart Parkin, Jammie Kaufman at IBM Almaden Research Center; John Slonczewski, Bill Gallagher, Arunava Gupta, Lia Krusin-Elbaum, Peter Duncombe, Bob Laibowitz, Daniel Lopez, John Kirtley, Chang Tsuei, Roger Koch, Robin Altman, Steve Brown, John Connolly at IBM Research Yorktown Heights; Dan Lathrop, Rob Matthews and Steve Haupt from Quantum Magnetics Inc.; Xinwei Li, G. Q. Gong, Yu Lu and Gang Xiao from Brown University for helpful discussions and for assistance at various stages of the experiment.

Appendix A. On fitting using Simmons's tunnelling model

Simmons's description (Simmons 1963*a–c*; Wolf 1989) of tunnelling I–V with symmetrical barrier can be written as

$$J(V,t,\phi)=\eta[(\phi-\tfrac{1}{2}qV)\mathrm{e}^{-A(\phi-qV/2)^{1/2}}-(\phi+\tfrac{1}{2}qV)\mathrm{e}^{-A(\phi+qV/2)^{1/2}}], \tag{A 1}$$

where

$$\eta=\frac{q}{2\pi ht^2}$$

and

$$A=\frac{4\pi t}{h}(2m)^{1/2}$$

with barrier thickness t, barrier height ϕ, and electron charge q. Many people (Miyazaki *et al*. 1997; Julliere 1975; Moodera *et al*. 1995; Maekawa & Gäfvert 1982; Nowak & Rauluszkiewica 1992; Platt *et al*. 1996) have used equation (A 1) to fit experimental data, and extracted t and ϕ. There is a danger in the literal interpretation of such t and ϕ, especially when inhomogeneities are present.

To model a real experimental junction, one often has to consider both parallel shunts and a decrease of effective tunnelling area. Assume the tunnelling portion of the current is described by equation (A 1), the apparent junction I–V characteristic can be expressed as

$$I(V,t,\phi)=\kappa J(V,t,\phi)+sV, \tag{A 2}$$

where $\kappa\leqslant 1$ describes the reduction of effective tunnelling area because of barrier thickness non-uniformities, and s describes the parasitic conductance brought forth by shunts (assumed to be ohmic for simplicity).

There is little difference in the appearance of equation (A 2) compared to equation (A 1). In fact they are equivalent in functional form up to $O(V^5)$. Thus a two-parameter fit to equation (A 1) will always give a reasonable fit to the first order, but with modified fitting parameters t,ϕ. The problem is, these t,ϕ do not have the same physical meaning as they do in the Simmons model equation (A 1).

To see this let us create a situation where a real junction can be represented by an ideal Simmons junction with $t_\mathrm{o},\phi_\mathrm{o}$ defined according to equation (A 1). Assume the real junction has parasitic κ and s and its I–V can be described by equation (A 2). What happens if we use the ideal junction formula, equation (A 1), to fit the real junction's IV as defined by equation (A 2)? The fit will give an apparent t,ϕ described by the minimization condition of

$$E_r=\int_{-V_\mathrm{o}}^{V_\mathrm{o}}[J(V,t,\phi)-I(V,t_\mathrm{o},\phi_\mathrm{o})]^2\,\mathrm{d}V, \tag{A 3}$$

where V_o is the voltage range of measurement.

At low-bias equation (A 1) can be expanded to $O(V^5)$ to give

$$J(V,\alpha,\gamma)=\alpha V+\gamma V^3+O(V^5), \tag{A 4}$$

where

$$\left.\begin{aligned}\alpha(t,\phi)&=\tfrac{1}{2}\eta q\mathrm{e}^{-A\sqrt{\phi}}(A\sqrt{\phi}-2),\\ \gamma(t,\phi)&=\tfrac{1}{192}\eta q^3\mathrm{e}^{-A\sqrt{\phi}}\frac{A}{\phi^{3/2}}(A^2\phi-3A\sqrt{\phi}-3).\end{aligned}\right\} \tag{A 5}$$

Since equation (A 1) is equivalent to equation (A 4) to $O(V^5)$, it is easy to see that the minimization of equation (A 3) leads to

$$\gamma = \kappa\gamma_{\rm o}, \qquad \alpha = \kappa\alpha_{\rm o} + s, \tag{A 6}$$

with $\alpha_{\rm o}$ and $\gamma_{\rm o}$ defined by $t_{\rm o}, \phi_{\rm o}$ through equation (A 5). So the real junction will also fit the ideal Simmons model equation (A 1) reasonably well, but with an off-set to parameters α, γ, thus to t, ϕ. It is therefore very misleading to use the definition of equation (A 1) to interpret t, ϕ and infer from this anything about the barrier height and barrier thickness.

What makes matters worse is that such fits based on equation (A 1) seem to give reasonable values for t, ϕ. The reason behind this is the strongly exponential dependence of the apparent conductance on $A\sqrt{\phi}$ in equation (A 1). Many nonlinear odd-function I–V characteristics can be expanded to V^3 and be assigned an α to the junction conductance s. An s thus defined would give a value to $A\sqrt{\phi}$ according to equation (A 5). Assume $\kappa = 1$ for simplicity,

$$\mathrm{e}^{-A\sqrt{\phi}} = \frac{2}{A\sqrt{\phi} - 2}\left(\frac{s}{\eta q}\right). \tag{A 7}$$

The value of

$$\eta q = \frac{q^2}{2\pi h t^2} = 6.2 \times 10^{14}\left(\frac{\text{Å}}{t}\right)^2 \Omega\,\mathrm{m}^2$$

is large compared to typical conductance s (usually around $10^6\ \Omega\,\mathrm{m}^2$) for any reasonable barrier thickness t, therefore it is self-consistent to assume a large $A\sqrt{\phi}$ limit. There the dependence of $A\sqrt{\phi}$ on s is logarithmic,

$$A\sqrt{\phi} = \ln\left(\frac{\eta q}{s}\right) + \ln\left(\frac{A\sqrt{\phi} - 2}{2}\right) \approx \ln\left(\frac{\eta q}{s}\right) \tag{A 8}$$

and to the first order self-consistently gives

$$t\sqrt{\phi} = \frac{h}{4\pi\sqrt{2m}}\left[\ln\left(\frac{1}{2}\frac{q^2}{\pi h s t^2}\right) + \ln\left(2\pi\frac{t}{h}\sqrt{2m\phi} - 1\right)\right] \sim \frac{\xi h}{4\pi(2m)^{1/2}}, \tag{A 9}$$

where ξ is a numerical factor around $10 \sim 20$, related to a reasonable thickness estimate by

$$\xi \approx 2\ln\left(\frac{q}{t\sqrt{2\pi h s}}\right). \tag{A 10}$$

Take our experiment for example. Our $s \approx 10^6\ \Omega\,\mathrm{m}^2$, a reasonable range would be $t \sim 30$ Å, or $\xi \sim 13$.

This can also be observed by numerically evaluating equation (A 9). To do so we define $t = t_1 \times 10^{-10}$ m, $\phi = \phi_1 q$ J, and using $h = 6.626 \times 10^{-34}$ J s, $q = 1.602 \times 10^{-19}$ C, $m = 9.31 \times 10^{-31}$ kg, $s = 10^6\ \Omega\,\mathrm{m}^2$, we have for t_1 in Å and ϕ_1 in eV,

$$t_1\sqrt{\phi_1} = 19.541 - 1.9309\ln t_1 + 0.96547\ln(0.51791 t_1\sqrt{\phi_1} - 1.0),$$

that gives

$$t_1\sqrt{\phi_1} \sim 16\ \text{Å}\ \mathrm{eV}^{1/2}, \tag{A 11}$$

which sets one constrain. A specific set of t, ϕ is then obtained by moving along this constrain (to satisfy linear conductance value) until it finds an approximate descrition for the leading nonlinear term as described by $\gamma = \kappa\gamma_o$ in equation (A 6). Different junctions and samples may have different ratio for first- and third-order expansion coefficients, which leads to a set of apparent t, ϕ that scatters roughly along the constrain equation (A 9). This is what we saw from our experimental fits, as shown in figure 14.

So be very careful when using Simmons's formula to fit experimental I–V curves. If there is inhomogeneity or parallel shunt conductances present, the apparent barrier height and thickness do not represent the values for the tunnelling barrier.

References

Anderson, P. W. & Hasegawa, H. 1955 *Phys. Rev.* **100**, 675.

Asano, Y., Oguri, A. & Maekawa, S. 1993 *Phys. Rev. B* **48**, 6192.

Asano, Y., Oguri, A., Inoue, J. & Maekawa, S. 1994 *Phys. Rev.* B **49**, 12831.

Chazalviel, J.-N. & Yafet, Y. 1977 *Phys. Rev.* B **15**, 1062.

de Gennes, P.-G. 1960 *Phys. Rev.* **118**, 141.

Dieny, B., Speriosu, V. S., Parkin, S. S. P., Gurney, B. A., Wilhoit, D. R. & Mauri, D. 1991 *Phys. Rev.* B **43**, 1297.

Doudin, B., Redmond, G., Gilbert, S. E. & Ansermet, J.-Ph. 1997 *Phys. Rev. Lett.* **79**, 933.

Gallagher, W. J., Parkin, S. S. P., Lu, Yu, Bian, X. P., Marley, A., Altman, R. A., Rishton, S. A., Roche, K. P., Jahnes, C., Shaw, T. M. & Xiao, G. 1996 *J. Appl. Phys.* **81**, 3741.

Goodenough, J. B., Wold, A., Arnott, R. J. & Menyuk, N. 1961 *Phys. Rev.* **124**, 373.

Gupta, A., Gong, G. Q., Xiao, G., Duncombe, P. R., Trouilloud, P., Lecoeur, P., Wang, Y. Y., Dravid, V. P. & Sun, J. Z. 1996 *Phys. Rev.* B **54**.

Hertz, J. A. & Aoi, K. 1973 *Phys. Rev.* B **8**, 3252.

Hwang, H. Y., Cheong, S.-W., Ong, N. P. & Batlogg, B. 1996 *Phys. Rev. Lett.* **77**, 2041.

Jin, S., Tiefel, T. H., McCormack, M., Fastnacht, R. A., Ramesh, R. & Chen, L. H. 1994*a* *Science* **264**, 413.

Jin, S., McCormack, M., Tiefel, T. H. & Ramesh, R. 1994*b* *J. Appl. Phys.* **76**, 6929.

Ju, H. L., Gopalakrishnan, J., Peng, J. L., Li, Q., Xiong, G. C. & Greene, T. Venkatesan, R. L. 1995 *Phys. Rev.* B **51**, 6143.

Julliere, M. 1975 *Phys. Lett.* **54A**, 225.

Kimura, T., Tomioka, Y., Kuwahara, H., Asamitsu, A., Tamura, M. & Tokura, Y. 1996 *Science* **274**, 1698.

Lu, Y., Li, X. W., Gong, G. Q., Xiao, G., Gupta, A., Lecoeur, P., Sun, J. Z., Wang, Y. Y. & Dravid, V. P. 1996 *Phys. Rev.* B **54**, R8357.

Maekawa, S. & Gäfvert, U. 1982 *IEEE Trans. Magn.* **MAG-18**, 707.

Maekawa, S., Inoue, J. & Itoh, H. 1996 *J. Appl. Phys.* **79**, 4730.

Mathur, N. D., Burnell, G., Issac, S. P., Jackson, T. J., Teo, B.-S., MacManus-Driscoll, J. L., Cohen, L. F., Evetts, J. E. & Blamire, M. G. 1997 *Nature* **387**, 266.

Matsuyama, K., Asada, H., Miyoshi, H. & Taniguchi, K. 1995 *IEEE Trans. Magn.* **31**, 3176.

McCormack, M., Jin, S., Tiefel, T. H., Fleming, R. M., Philips, J. M. & Ramesh, R. 1994 *Appl. Phys. Lett.* **64**, 3045.

Meservey, R. & Tedrow, P. M. 1993 *Phys. Rep.* **238**, 173.

Millis, A. J. 1996 *Phys. Rev.* B **53**, 8434.

Millis, A. J., Shraiman, B. I. & Mueller, R. 1996 *Phys. Rev. Lett.* **77**, 175.

Miyazaki, T. & Tezuka, N. 1995*a* *J. Magn. Magn. Mat.* **139**, L231.

Miyazaki, T. & Tezuka, N. 1995*b* *J. Magn. Magn. Mat.* **151**, 403.
Miyazaki, T., Tezuka, N. & Kumagai, S. 1997 *Physica* B **237–238**, 256.
Moodera, J. S., Kinder, L. R., Wong, T. M. & Meservey, R. 1995 *Phys. Rev. Lett.* **74**, 3273.
Moodera, J. S., Kinder, L. R., Nowak, J., LeClair, P. & Meservey, R. 1996 *Appl. Phys. Lett.* **69**, 708.
Mott, N. F. 1969 *Phil. Mag.* **19**, 835.
Nowak, J. & Rauluszkiewica, J. 1992 *J. Magn. Magn. Mater.* **109**, 79.
Pedersen, R. J. & Vernon, F. L. 1967 *Appl. Phys. Lett.* **10**, 29.
Pickett, W. E. & Singh, D. J. 1996 *Phys. Rev.* B **53**, 1146.
Platt, C. L., Dieny, B. & Berkowitz, A. E. 1996 *Appl. Phys. Lett.* **69**, 2291.
Roder, H., Zang, J. & Bishop, A. R. 1996 *Phys. Rev. Lett.* **76**, 1356.
Simmons, J. G. 1963*a* *J. Appl. Phys.* **34**, 238.
Simmons, J. G. 1963*b* *J. Appl. Phys.* **34**, 1793.
Simmons, J. G. 1963*c* *J. Appl. Phys.* **34**, 2581.
Simmons, J. G. 1964 *J. Appl. Phys.* **35**, 2655.
Slonczewski, J. 1976 *IBM Tech. Disclosure Bull.* **19**, 2328–2330.
Slonczewski, J. C. 1989 *Phys. Rev.* B **39**, 6995.
Steenbeck, K., Eick, T., Kirsch, K., O'Donnell, K. & Steinbeiß, E. 1997 *Appl. Phys. Lett.* **71**, 968.
Sun, J. Z. 1997 Manganate trilayer junctions: spin-dependent transport and low-field magnetoresistance. In *Colossal magnetoresistance oxides* (ed. Y. Tokura). Gordon and Breach.
Sun, J. Z., Gallagher, W. J., Duncombe, P. R., Krusin-Elbaum, L., Altman, R. A., Gupta, A., Lu, Yu, Gong, G. Q. & Xiao, G. 1996 *Appl. Phys. Lett.* **69**, 3266.
Sun, J. Z., Krusin-Elbaum, L., Duncombe, P. R., Gupta, A. & Laibowitz, R. B. 1997 *Appl. Phys. Lett.* **70**, 1769.
Suzuki, Y., Hwang, H. Y., Cheong, S.-W. & Dover, R. B. Van 1997 *Appl. Phys. Lett.* **71**, 140.
Von Helmolt, R., Wecker, J., Holzapfel, B., Schultz, L. & Samwer, K. 1993 *Phys. Rev. Lett.* **71**, 2331.
Wolf, E. L. 1989 In *Principles of electron tunneling spectroscopy*, p. 37. Oxford, New York: Oxford University Press.
Wollan, E. O. & Koehler, W. C. 1955 *Phys. Rev.* **100**, 545.
Zhang, S., Levy, P. M., Marley, A. C. & Parkin, S. S. P. 1997 *Phys. Rev. Lett.* **79**, 3744.

Discussion

T. T. M. Palstra (*University of Groningen, The Netherlands*). What materials would be good for trying as other barriers?

J. Z. Sun. You probably want a good lattice match to ensure that you are not disrupting the LSMO too much. We have tried quite a few (CeO, MgO, $LaAlO_3$), but it also has to be something which we can easily grow in a very uniform way, up to 30 Å, which is by itself very hard to characterize. We have gone through a first pass and none of them come out as good as $SrTiO_3$: MgO is full of pin-hole shorts; with CeO, the MR does not seem to be as big; with $LaAlO_3$, we have seen some large MRs, but not as reproducibly as with $SrTiO_3$, but at least it's better than the others.

J. E. Evetts (*University of Cambridge, UK*). Dr Sun has a relatively large number of devices on a single chip, and they seem quite close together, so this means there is probably magnetic coupling between the different devices. He may find that he

gets systematic differences when he moves to an edge of the whole chip. He will get a different domain structure or different magnetic response from when he's in the middle.

J. Z. Sun. Yes and no; the devices are not actually that close if you think about it in terms of the top pillar. They are 1–2 μm in size and about 200 μm apart to say the least. There might be some coupling, but so far it's so noisy and random that we haven't seen that on the chip level there is any correlation.

J. M. D. Coey (*Trinity College, Dublin, Ireland*). Did Dr Sun measure the conductance below 4 K to see whether there really is a Coulomb gap?

J. Z. Sun. No, we haven't cooled it down below 4 K.

J. R. Cooper (*University of Cambridge, UK*). In 1969 I worked as a postdoc with Adrian Wyatt in the UK. We used to have Al layers oxidized and then we had a shutter and we used to evaporate less than a monolayer of all the 3d transition elements on to the oxide barrier. We then used to cover it either with Al or silver. It is well documented in the old literature that there are two effects: there is a so-called resistance peak, which we never understood, and a resistance minimum, which is the Kondo effect. The resistance peak came from transition metal impurities and it did vary with the transition metal, and, as I remember, it went as the square of the concentration. So, my comment is that perhaps Dr Sun should think of trying to cut down on the manganese, because it was the Mn which did it. The weird effects came from having Mn atoms in the oxide, so I would reduce the Mn concentration a bit to avoid having any free Mn.

J. Z. Sun. Is it essential to have magnetic moment? It is more like a Coulomb gap.

J. R. Cooper. No, I only remember it vaguely. We saw if there was a magnetic moment from the Kondo effect, but the resistance effect came with or without a magnetic moment.

PHILOSOPHICAL TRANSACTIONS OF THE ROYAL SOCIETY A MATHEMATICAL, PHYSICAL & ENGINEERING SCIENCES